Geomorphic process fingerprints in submarine canyons

Daniel S. Brothers, Uri S. ten Brink, Brian D. Andrews, Jason D. Chaytor, David C. Twichell*

Woods Hole Coastal and Marine Science Center

US Geological Survey

384 Woods Hole Rd

Woods Hole, MA 02559

*Corresponding author: dbrothers@usgs.gov; 508-457-2293

Abstract

Submarine canyons are common features of continental margins worldwide. They are conduits that funnel vast quantities of sediment from the continents to the deep sea. Though it is known that submarine canyons form primarily from erosion induced by submarine sediment flows, we currently lack quantitative, empirically based expressions that describe the morphology of submarine canyon networks. Multibeam bathymetry data along the entire passive US Atlantic margin (USAM) and along the active central California margin near Monterey Bay provide an opportunity to examine the fine-scale morphology of 171 slope-sourced canyons. Log-log regression analyses of canyon thalwag gradient (S) versus up-canyon catchment area (A) are used to examine linkages between morphological domains and the generation and evolution of submarine sediment flows. For example, canyon reaches of the upper continental slope are characterized by

steep, linear and/or convex longitudinal profiles, whereas reaches farther down canyon have distinctly concave longitudinal profiles. The transition between these geomorphic domains appears to be dependent on catchment area, which may be a proxy for sediment supply, and is inferred to represent the downslope transformation of debris flows into turbidity flows. The morphology of slope-sourced canyon heads may provide insights into the conditions needed to generate erosive, canyon-flushing turbidity flows.

Keywords: turbidity flow, debris flow, multibeam bathymetry, regression, power law, landslide

1. Introduction

The geomorphic evolution of continental margins and, in particular, the formation of submarine canyons is heavily influenced by the interplay between sedimentary mass flows and seafloor topography (Mitchell, 2005; Ramsey et al., 2006; Gerber et al., 2009; Paull et al., 2013). However, direct observations of dynamic erosion from sediment flows are rare (Paull et al., 2003; Xu et al., 2004) and our understanding of canyon erosion mechanisms is based largely on laboratory and analytical inferences (Kneller and Buckee, 2000; Mohrig and Marr, 2003; Gerber et al., 2009). Many of the principal studies aimed at understanding the origins and evolution of submarine canyons were either focused on a select number of the large, predominantly shelf-sourced canyon systems (Shepard and Emery, 1973; Farre et al., 1983; Gardner, 1989; Piper and Savoye, 1993; Greene et al., 2002; Pirmez and Imran, 2003; Puig et al., 2004; Paull et al., 2011), or on a mixture of

shelf- and slope-sourced canyons having relatively limited spatial extent and bathymetric resolution (Shepard, 1981; Pratson et al., 1994; Pratson and Coakley, 1996; Mitchell, 2004, 2005; Ramsey et al., 2006; Straub et al., 2007; Paull et al., 2011; Paull et al., 2013). Slope-sourced canyons are assumed to be fully decoupled from onshore drainage systems, whereas the larger and older shelf-sourced canyons that extend shoreward of the classically defined shelf-edge (Kennett, 1982). To study the linkages between form and process, these two classes of submarine canyons should be studied separately because they evolve under fundamentally different boundary conditions and perhaps over very different time-scales (Twichell and Roberts, 1982; Farre et al., 1983).

In this study, we explore the relationship between channelized mass flows and the development of submarine canyon network morphology using an enormous volume of continuous, high-resolution bathymetric data from two separate settings: the US Atlantic and Central California continental margins (Figure 1). Our aim is to address the following fundamental questions: (1) is there an objective way to define the head-ward extent of submarine canyon networks? (2) Do submarine canyon networks have consistent and predictable patterns regardless of setting? (3) Can we use canyon network scaling relations to identify different process domains that relate to the dynamic behavior of submarine sediment flows?

2. Submarine Mass Flows and Canyon Network Morphology

The dominant process responsible for submarine canyon formation is the tendency of sediment flows to channelize into avenues of concentrated erosion (Pratson and Coakley, 1996). Submarine landslides generated by failure of unstable sediments in

and around canyon heads and along steep canyon walls can accelerate and entrain water as they move downslope and can transform into erosive turbidity flows (Hampton, 1972; Mohrig et al., 1998; Piper et al., 1999; Mohrig and Marr, 2003). Over time, repeated turbidity flows erode networks of canyons across the continental slope and rise whose bathymetric expressions resemble topography of terrestrial channel networks (Belderson and Stride, 1969; Mcgregor et al., 1982; Twichell and Roberts, 1982; Pratson and Coakley, 1996; Mitchell, 2005).

Terrestrial researchers have created conceptual and theoretical models to describe the evolution of drainage basins and to delineate geomorphic process domains. Hillslopes and stream valleys represent the most significant features in terms of drainage basin evolution (Willgoose et al., 1991b, a; Tucker and Bras, 1998; Whipple and Tucker, 2002; Stock and Dietrich, 2003). Hillslope domains tend to be located in and around channel heads and near drainage divides. They are characterized by soil creep, debris flows and landslides across topographic surfaces having relatively steep gradients and small catchment areas (Howard, 1994). In contrast, stream valley domains appear below hillslope domains and their morphology is dominated by erosion due to overland flow. Stream-bed shear stresses increase with flow discharge and/or thalwag gradient. When high-quality topographic data is available, drainage area is commonly used as a proxy for stream discharge, therefore the magnitude of stream bed shear stress at a given location can be defined as a function of catchment area and local thalwag gradient (Seidl and Dietrich, 1992; Tucker and Bras, 1998; Whipple and Tucker, 2002; Wobus et al., 2006).

A standard approach in fluvial geomorphology is to measure the local thalwag gradient (S) and the associated catchment area (A) at discrete points along a longitudinal

channel profile (e.g., Kirby and Whipple, 2001). The transport capacity, Q_s, of a stream channel can then be approximated as a power function of A and S (Howard [1994]; references therein):

$$Q_s = KA^m S^n \qquad \textbf{(1)}$$

where K, m and n are constants. In a steady state landscape, Q_s is balanced by the tectonic uplift rate, U, and the long-term sediment transport through any location must equal the product of uplift rate and contributing drainage area. Equation (1) can be rearranged into a generalized form relating catchment area to local thalwag gradient (Tucker and Whipple, 2002; references therein):

$$S = K_s A^{-\theta_i} \qquad \textbf{(2)}$$

K_s and θ_i are the channel steepness (m/m) and intrinsic concavity indices, respectively. Segments of an individual stream profile characterized by different values for θ_i and/or K_s are often used to identify downstream thresholds of process dominance (Howard, 1994; Tucker and Bras, 1998) and to examine the responses of landforms to tectonic uplift and climate change (Whipple and Tucker, 2002). Both parameters are estimated by applying least squares regression to log-log scatter plots of A versus S: θ_i is the slope of the regression curve and K_s is the y-intercept. For example, the first kink in S-A regression plots (small A and large S; Figure 2) is widely interpreted to represent a geomorphic threshold separating landscapes that are dominated by hillslope processes from those

dominated by fluvial incision and valley formation (Tucker and Bras, 1998; Stock and Dietrich, 2003). Hillslope domains tend to have linear or convex longitudinal profiles ($\theta_i < 0$) whereas stream valleys have concave profiles (θ_i typically ranges between 0.3 – 0.6), meaning the thalwag gradient decreases exponentially with increasing area. The threshold separating these domains typically occurs where the drainage area exceeds ~10^6 m^2 (Tucker and Whipple, 2002). Additional thresholds in the *S-A* plots that occur at larger drainage areas and have been linked with changes in fluvial sediment transport capacity, such as the transition from supply limited to transport limited domains (Whipple and Tucker, 2002; Figure 2).

In the marine realm, the uppermost continental slope is often characterized by steep, convergent topography associated with submarine canyon heads. Sediment movement in and around canyon heads and along inter-canyon ridges is dominated by diffusive transport and small-scale landsliding (Pirmez et al., 1998; Mitchell and Huthnance, 2007). Seabed observations suggest that canyon heads contain pervasive evidence for retrogressive failures, debris flow deposits and steep, narrow gullies that converge downslope into deeply entrenched canyon valleys. Canyon valleys are thought to form primarily by turbidity current erosion. However, few studies have investigated the morphological connection between retrogressive failures in and around slope-sourced canyon heads and the generation of turbidity flows that scour and erode canyon valleys of the continental slope (Twichell and Roberts, 1982; Farre et al., 1983; Pratson et al., 1994; Piper and Normark, 2009). Canyon relief generally diminishes along the lowermost slope/upper rise where mass flow deposition and aggradation of leveed channels systems begin to dominate (Galloway, 1998).

Within the context of slope depositional systems, submarine canyon networks can be segregated based on the primary source of the sediment transported down canyon (i.e., allocthonous versus autochtonous systems). The shelf-edge delineates a major hydrographic boundary separating wave and current driven sediment transport on the shelf from gravity driven transport of the slope (Pirmez et al., 1998). We define shelf-sourced canyons as those that extend landward of the continental shelf-break and have higher propensity to capture sediment transported by shelf processes and/or by direct connections to terrestrial drainage systems (Shepard and Emery, 1973; Shepard, 1981; Mulder and Syvitski, 1995; Johnson et al., 2001). In contrast, slope-sourced canyons have heads located along the uppermost continental slope and are assumed to evolve primarily from erosion induced by local slope failures and mass flows sourced from within the canyon network (Twichell and Roberts, 1982; Pratson et al., 1994; Pratson and Coakley, 1996; Goff, 2001; Brothers et al., 2013). Hypothetical drainage divides for slope-sourced canyon networks can be delineated along the uppermost slope. We assume that sediment entering canyon networks is sourced from within the network, then carefully extract and analyze the canyon network morphology using a geomorphic framework developed by terrestrial studies.

Previous studies used digital elevation models (DEMs) derived from multibeam bathymetry data to examine the *S-A* scaling parameters, longitudinal thalwag profiles and erosion processes in submarine canyons, but yielded mixed results (Pratson and Ryan, 1996; Mitchell, 2005; Ramsey et al., 2006; Straub et al., 2007). Mitchell (2005) observed an inverse power-law relationship in *S-A* regression plots and developed an erosion model in which hemipelagic sediments accumulate on the walls of canyons until they

become unstable and initiate erosive sedimentary flows. It was speculated that a steady-state canyon configuration develops due to a balance between slope aggradation and canyon entrenchment. The frequency and size of erosive flows increases down-canyon, which increases cumulative erosion in a way that is analogous to increased stream discharge with drainage area in fluvial geomorphology.

3. Methods

We apply DEM-based geomorphic analysis (e.g., Wobus et al., 2006) to an enormous volume of multibeam bathymetry data from both passive and active margin settings. Along the passive USAM, bathymetric data were collected during 26 separate geophysical cruises covering approximately 616,000 km^2 of the slope and rise between Georges Banks and the Blake Plateau (Figure 1a, c; Andrews et al., 2013; Brothers et al., 2013). We used a continuous 100-m resolution DEM for most of the quantitative analysis, but several sub-regions along the upper slope were gridded at 10 and 25 m for detailed qualitative interpretations of canyon head morphology. Along the active central California margin, significant along-strike tectonic variation occurs (Greene et al., 2002), so our analysis was limited to a 7,500 km^2 region located to the southwest of Monterey Bay, just offshore of the Sur Platform (Figure 1b, d). Multibeam bathymetry data (Hatcher et al., 2000; Greene et al., 2002; Wong and Eittreim, 2002) were gridded at 25-m for quantitative analysis and 5-m for detailed qualitative interpretations of outer shelf and upper slope morphology.

Because slope-sourced canyon heads are located at variable depths below the shelf-edge, using a single bathymetric contour to define the upper-slope drainage divides

(Mitchell, 2005; Straub et al., 2007) may lead to incorrect estimates of canyon head catchment areas. A hypothetical uncanyonized DEM was constructed by interpolating a surface across the crests of canyon interfluves and inter-canyon plains of the outer shelf and slope. This surface also allowed us to examine the first-order shape of the uncanyonized continental slope, or "interfluve" surface (Brothers et al., 2013). Canyon relief was defined as the relative elevation difference between the canyon thalwag and the hypothetical uncanyonized surface. In other words, relief is measured from the thalwag to the crest of the adjacent inter-canyon ridges. Drainage divides along the uppermost continental slope were interpreted based on fine-scale canyon head morphology and local bathymetric relief. Canyon head relief was used to guide manual selection of drainage divides along the outer shelf and uppermost continental slope (e.g., Figure 3); drainage divides were selected where relief along the upper rim of canyon heads exceeded 10-m. Uncertainties associated with drainage divide selection are estimated to produce errors in catchment area of less 0.5 km^2. Next, using the hypothetical drainage divides, bathymetric DEMs were split into drainage basins using flow accumulation arrays and watershed analysis tools in ARC/INFO. Initially, all submarine canyons and channels were extracted from the bathymetric DEMs (Figures 1c,d) and used to differentiate between shelf-sourced and slope-sourced canyons in each study region.

Thalwag depth, gradient (S), canyon relief and catchment area (A) were extracted at every 20 m contour down the thalwag of each slope-sourced canyon. Because of the similarities between fluvial drainages and submarine canyon networks, we assumed from the beginning that canyon network morphology can be described by power-law scaling relations between gradient and catchment area and did not perform sensitivity analysis

aimed at testing other empirical models. Regression analysis was applied to *S-A* scatter plots of each individual canyon for a total of 120 canyons along the USAM and 51 canyons along the Sur Platform. The regression analysis of log-log *S-A* scatter plots involved a certain degree of inherent subjectivity because the limits for each fit were selected manually across groupings of points that appeared to follow a linear trend for at least one order of magnitude in either catchment area or gradient. Picks were guided by a log-binned running average of *S-A* points in an effort to reduce subjective bias in the identification of distinctive linear segments (e.g., Figure 4; Wobus et al., 2006). A measure of variance (R^2) was computed for each regression segment within each individual canyon. Estimates for θ_i along each regression segment and the *S-A* values for segment boundaries for each individual canyon were saved to a database. Basic statistics were computed for all segments identified along both margins (Table 1). Interpretations were based on correlations between distinct regression segments and geologic features identified within specific reaches of submarine canyons.

4. Results

4.1. S-A analysis of slope-sourced canyons

Examples of characteristic canyon profiles and their associated *S-A* regression analyses are shown in Figures 4 and 5. To first-order, the log-log plots of *S-A* data for each of the slope-sourced canyons on both margins display patterns that are similar to those observed in terrestrial drainage networks (Figure 2). Regression analysis suggests USAM canyons exhibit an average of four distinctive concavity segments and Sur Platform canyons are characterized by two measureable segments, plus a third segment

along the lowermost slope that was not measured due to its extreme variation and convexity. The steepest segments of canyon profiles are located along the uppermost continental slope. Regression analysis of these segments yield concavity estimates that are approximately zero ($\theta_i \simeq 0$) or slightly negative ($\theta_i < 0$), meaning the associated longitudinal profiles are either linear or slightly convex (Figures 4 and 5). Some canyons contain a short convex segment just below the drainage divide that becomes linear farther downslope (e.g., Figure 5). An abrupt transition in θ_i is observed on both margins and marks the change from linear/convex to highly concave profiles ($\theta_i > 0$). For descriptive purposes (see Discussion for explanations) we apply the following nomenclature to distinguish between segments. The steep, canyon segments located immediately below the drainage divides and characterized by convergent topography are considered to be within the "landslide" domain, the transition between linear/convex and concave canyon profiles (intersection of the two regression lines) will be called "threshold-1", and the concave segments below threshold-1 are associated with the "canyon-valley" domain (Figures 4 and 5). The scaling parameters estimated for each regression segment within each individual canyon were averaged to produce composite *S-A* power-law functions (Figure 6) and to identify physical parameters associated with boundaries between different segments.

Threshold-1 was relatively straightforward to identify for almost every canyon (e.g., Figures 4–6). *S-A* values for threshold-1 (termed S_t and A_t) were manually picked from individual plots of each canyon. We estimate the average uncertainty in S_t and A_t picks to be less than 10%. For the USAM (Figure 6a): S_t ranges from 2.9°–10.1° and has a median value of 7.3°; A_t ranges from 1.8 km^2–128.1 km^2 with a median of 8.8 km^2. For

Sur Platform canyons (Figure 6b): S_t ranges from 5.1°–23.7° with a median value of 11.3°; A_t ranges from 0.1 km^2–8.5 km^2 with a median of 0.4 km^2. A log-log scatter plot of threshold-1 values (Figure 6c) reveals distinct distributions for the separate margins, but also an overall trend consistent with both datasets. The USAM data spans greater catchment areas and smaller gradients, whereas the Sur Platform data spans small areas and gradients. A combined fit yields an interesting trend in which the gradient decreases exponentially with increasing area in the form of $S_t=2.09A_t^{-0.18}$ ($R^2=0.69$).

Seafloor morphology within the landslide domains of both margins is dominated by gullies, debris flow channels and irregular surfaces associated with sinuous failure scarps (10–20 m high; Figure 7). Such features lead to considerable variation in S and result in relatively low R^2 values (0.4 – 0.5 on average) in the regression analyses. Along the USAM, small pockmarks (100–200 m diameter) cover the seafloor surrounding the landslide domain (Figure 7a), particularly along the uppermost continental slope. Canyon segments located within the landslide domains occur between the shelf-edge and water depths up to 1600 m and vary in length depending on the geometry of the catchment above threshold-1 (Figures 5–8). Narrow landslide catchments appear to be associated with longer canyon segments that extend to greater depths than the wider, shorter catchments. However, the area of individual landslide domains does not appear to be related to shape (Figure 5). The average thalwag gradient of canyons and gullies within the landslide domain is 10.2° ± 1.8°. More than 70% of the total terrain located within landslide catchment areas is steeper than 8° and more 95% of the terrain is steeper than 5°.

In contrast, along the Sur Platform the average gradient of canyon thalwags within the landslide domain is 13.5° ± 3.7°. Segments are relatively short and extend from the shelf edge down to a maximum depth of ~400 m (e.g., Figures 4 and 7b). The seafloor along canyon walls contains fewer gullies and landslide scars than the USAM canyons, but the steep slopes near canyon heads show evidence for slope failures. Canyon heads are separated from the shelf break by a scarp at ~160-m depth. The terraced appearance of the shelf break is associated with exposed, more resistant substrate (Eittreim et al., 2002).

Canyon relief generally increases downslope as narrow gullies within the landslide domain converge and transition into canyon-valley domains located downslope of threshold-1. The canyon-valley segments can be fit relatively well by an inverse power-law ($\theta_i > 0$), despite typically convex shapes of the adjacent canyon interfluves (e.g., Figure 4). The canyon-valley domains of the USAM canyons contain three primary regression segments with average concavities of $\theta_{iA1} = 0.65 \pm 0.06$, $\theta_{iA2} = 0.39 \pm 0.07$ and $\theta_{iA3} \leq 0.1$. Average R^2 values for θ_{iA1} segments range from 0.5–0.89, with an average of $R^2 = 0.65$. Regression of θ_{iA2} and θ_{iA23} are significantly worse, with R^2 values rarely exceeding 0.5 for either segment. However, much of the variation in θ_{iA1} and θ_{iA2} is related to outlier *S-A* data associated with canyon confluences, "knickpoints", and overprint from mass failures along the lower slope and upper rise. Sur Platform canyons have two segments that could be systematically measured using regression analysis. The mean values are $\theta_{iM1} \simeq 0.45 \pm 0.05$, $\theta_{iM2} \leq 0.1$ (Figure 4). Average R^2 values for θ_{iM1} segments range from 0.4–0.92, with an average $R^2 = 0.69$; R^2 values for θ_{iM2} are between 0.3–0.6 and, as noted, regression analysis of the lower slope reaches was not attempted

due to the extreme variation convexity. Simple comparison shows that $\theta_{iM1} \simeq \theta_{iA2}$ and $\theta_{iM2} \simeq \theta_{iA3}$.

Though a more comprehensive analysis is needed, canyons with larger catchment areas at threshold-1 appear to have higher concavities and higher relief along the first canyon-valley segment. Canyons reaches with gradients > 5° tend to have v-shaped cross-sections and those with gradients < 3° are often flat-bottomed or U-shaped. Off the Sur Platform, canyon gradients decrease to less than 5° within 2.5 km of threshold-1, whereas most of the USAM canyons drop below 5° between 5–12 km down canyon of threshold-1.

The segment of greatest intrinsic concavity along USAM canyons, θ_{iA1}, is confined to the continental slope and uppermost rise (Figure 8a–c). In general, the boundary between θ_{iA1} and θ_{iA2} appears to coincide with either the change in thalwag gradient or a drop-off in canyon relief associated with the slope-rise transition along the inter-canyon ridges. Across-canyon bathymetric profiles along θ_{iA1} are relatively narrow and bounded by steep walls (Figure 9a). They are mostly v-shaped between depths of about 500–1500 m, then become flat bottomed as they transition to θ_{iA2} canyon reaches along the lower slope and uppermost rise. θ_{iA3} segments begin along the continental rise in depths >2500 m and are associated with deep-sea channels. Channels that do not merge with major shelf-sourced canyon-channel systems are characterized by low relief and low gradients (<1°). Sediment waves, failure scars and landslide deposits characterize the surrounding seafloor (Figure 8a-c). Some channels appear to be infilled and their bathymetric expression disappears on the upper rise; others have subtle morphology that can be traced 10's of km seaward of the base of the slope.

Canyon reaches of the Monterey margin corresponding to concavity segment θ_{M1} are confined to the upper slope and many exhibit broad meanders. Cross-sections show mixed v-shaped and flat-bottomed profiles, with v-shaped profiles concentrated headward (Figure 9b). Interfluve longitudinal profiles are convex along the uppermost slope and then appear to parallel their adjacent canyon profiles across the middle slope (e.g., Figure 4b). Profiles of θ_{M1} canyon reaches show nearly constant channel gradients along θ_{M2} reaches, then the gradient increases rapidly to more than 10° as the θ_{M3} reach crosses the lower slope.

5. Discussion

Studies by Mitchell (2004; 2005) and Ramsey et al. (2006) provided compelling evidence that canyon network scaling relations can be used to identify process boundaries and to develop empirical erosions laws. In spite of this, subsequent modeling results suggested that erosion caused by channelized turbidity flows is not dependent on catchment area (Gerber et al., 2009) and that canyon morphology does not support a landslide driven connection to catchment area (Straub et al., 2007). These studies (Straub et al., 2007; Gerber et al., 2009) did not emphasize the genetic differences between the shelf-sourced and slope-sourced canyons that were used in their analyses and the resolution and spatial extent their data were relatively limited. Therefore, rejecting terrain network scaling relations in studies of submarine canyon evolution may be premature.

5.1. Implications of landslide domains and threshold-1

Valley incision by debris flows is an important process within the steep, upland reaches of terrestrial river networks (Stock and Deitrich, 2003). In regions with slopes steeper than ~0.10 (~5°), valley network incision is heavily influenced by debris flow scour and associated with curved log-log plots of *S-A* data. Abrupt transitions from debris flow mantled upland valleys to fluvially incised bedrock valleys are well documented (Stock and Deitrich, 2003). The transitions occur at catchment areas between 0.1 – 1 km^2 and are associated with distinctive breaks in the *S-A* scaling parameters (e.g., the transition between segments where $\theta_i \simeq 0$ to segments where $0.3 \leq \theta_i \leq 0.6$; Figure 2b). We present a similar scenario for the submarine environment, but our geomorphic interpretations are focused on the behavior of subaqueous debris flows and turbidity flows (e.g., Ramsey et al., 2006). We propose that debris flow incision dominates within the landslide domain of slope-sourced canyons and has an *S-A* signature distinct from that of canyon-valleys farther down slope. The scaling break separating the two domains may represent the critical point at which geomorphically significant debris flows (i.e., those that leave behind a lasting fingerprint) transform into turbidity flows.

Sediment released by slope failures is expected to accelerate, break up and transform into turbidity flows (Hampton, 1972). Once turbidity flows are generated, they can become self-accelerating through the entrainment of sediment and water, a process called ignition (Parker et al., 1986). Turbidity flows can erode, entrain and transport loose sediment along the canyon floor to deeper waters. One of the best-documented examples of this transformational process is along the Scotian margin of eastern Canada (Piper et al., 1999; Mosher and Piper, 2007; Piper and Normark, 2009), where it is hypothesized that the 1929 M7.2 Grand Banks Earthquake triggered widespread slope failure along the

continental slope. Like the USAM, the seafloor just below the shelf-edge contains little evidence for mass wasting, but instead is covered by pockmarks. The slope gradient rapidly increases in and around canyon heads (~500–700 m depth) and the pockmarks give way to failure scars and localized failure deposits. Farther downslope shallow channels and gullies converge into canyon-valleys that are devoid of debris flow deposits. Based on detailed seafloor observations, it is inferred that landslides and debris flows generated within the steep, head-ward reaches of submarine canyons evolved rapidly into turbidity flows, which in turn scoured and flushed loose material from canyon valleys out to deeper waters (Piper et al., 1999; Mosher and Piper, 2007; Piper and Normark, 2009). The debris flows appear to have transformed into turbidity flows in water depths between 700–1500 m, approximately the same depth range as threshold-1 along the USAM canyons. In general, the seafloor morphology and geologic history of the Scotian margin is comparable to that of the USAM.

The spatial association of steep, linear canyon profiles across the uppermost slope, and widespread evidence for sediment failures (e.g., Figure 7) suggests that mass wasting is the dominant process acting within the landslide domain. Failures along the upper slope imply that the linear and convex longitudinal canyon profiles within the landslide domain experience repeated failures between episodes of deposition and that the profile gradient fluctuates about a slope stability threshold (e.g., Figure 10) that may be controlled by local geotechnical parameters (Adams and Schlager, 2000). The convex shape of interfluve profiles between the shelf-edge and ~1000 m depths (e.g., Figures 4 and 5) suggests that shelf-edge and upper slope depocenters are primary sources of unstable sediment that is captured by steep canyon heads during failures.

Based on the similar structure of submarine canyons and fluvial channel networks (Figures 2 and 9) as well as the geomorphic and geologic similarities between the USAM and the Scotian margin, we propose that threshold-1 approximates the downslope transformation of debris flows and landslides into turbidity flows. Near threshold-1, sediment failures sourced from the steep slopes above ignite into erosive turbidity flows that flush canyon-valley segments, leading to entrenchment and the higher profile concavity across the slope and uppermost rise. Based on the range of S_t-A_t values associated with threshold-1 picks (Figure 6c), we infer that sediment failures on slope gradients less than 0.08 (~4.5°) are unlikely to generate erosive turbidity flows.

The distributions of Threshold-1 values for the USAM and Sur Platform canyons (Figure 6c) can be interpreted in several ways. The fact that we observe consistent and potentially predictable patterns in slope-sourced canyon morphology suggests these canyons owe their basic form to a common process that dominates over geological time scales. S_t and A_t values for the USAM and Sur Platform appear to define opposite ends of the same trend (Figure 6c). If the behavior of sediment flows passing through canyons is related to the landslide catchment area, it is possible that catchment area is a proxy for total volume of sediment mobilized during significant failure events, such those seismically triggered (Piper et al., 1999; ten Brink et al., 2009). The scatter about the regression fit (Figure 6c) may represent spatial differences in the material properties of unstable sediment (cohesion, lithology, shear strength) and/or differences in sediment accumulation since the most recent failure event (Tucker and Bras, 1998). All factors being equal (e.g., grain size and cohesion), the generation of a debris flow and its transformation into a turbidity flow depends on the flow momentum, which is a function

of the seabed gradient and the volume of failed sediment (Parker et al., 1986). IThe higher values for S_t along the Sur Platform may imply that flows accelerate more rapidly on steeper slopes and ignition occurs at smaller catchment areas relative to the USAM canyons. In this scenario, preexisting physiography has an important role in the behavior of sediment flows. For example, external forcing (e.g., tectonic uplift) may be responsible for the steepness of Sur Platform landslide segments.

On the other hand, the distinctive Threshold-1 distributions for the USAM and Sur Platform canyons may be caused by other factors that affect sediment flow dynamics, such as the cohesion/grain size of the failed sediment, the way flows are initiated and physiography of the continental shelf. The relatively narrow continental shelf, shallow shelf-edge and active tectonic deformation along the central California margin (Greene et al., 2002; Wong and Eittreim, 2002) is expected to have a profound influence on the nature of sediment shunted off the margin. The closer proximity of canyon heads to terrestrial sediment sources and shallow water oceanographic processes along the Sur Platform may lead to slope failures containing higher proportions of sand, but also the potential for flow initiation along the outer shelf above the canyon heads. Sediment flows containing higher sand content are expected to dissociate and entrain water more rapidly than flows containing high proportions of cohesive clay (Mohrig and Marr, 2003). It is possible that sandy, shelf-sourced sediment flows enter canyon heads with an initial velocity, and transform into turbidity flows at relatively small catchment areas. In this interpretation, our assumption that sediment flows are autogenically derived appears justified for the USAM canyons, but may not always be the case for the Sur Platform

canyons. Nonetheless, extensive core and near-bottom current data in slope-sourced canyon heads of both margins are needed to test between these interpretations.

5.2. Extracting flow properties from geomorphic scaling relations

Recent laboratory research has expanded on ideas and observations established early (e.g., Hampton, 1972; Middleton, 1966) regarding the conditions and mechanisms that cause debris flows to transform into turbidity flows (Mohrig and Marr, 2003). Few studies have attempted to quantify the geomorphic significance of canyon heads in terms of setting the boundary conditions for erosive, canyon-flushing turbidity flows. Initial thickness and flux are fundamental parameters needed for numerical and laboratory models of sediment flow dynamics (Hampton, 1972; Parker et al., 1986; Zeng and Lowe, 1997; Mohrig et al., 1998; Mohrig and Marr, 2003) and for models of submarine canyon erosion (Gerber et al., 2009). Based the inferred locations for major process boundaries, we develop an approach to constrain the critical thickness of geomorphically significant debris flows, d_c, at threshold-1 as a function of catchment area. To do this, we make several assumptions regarding sediment flow dynamics based on our results and early work by Hampton (1972): (1) threshold-1 marks the transformation of debris flows into turbidity flows, i.e., the transition from a laminar or near laminar density flow to a turbulent flow regime; (2) the stability of a debris flow of a particular size and velocity increases as a function of its yield strength (Hampton, 1972); (3) yield strength is exceeded and flows become turbulent when they exceed a critical velocity, however we do not make explicit assumptions about the physical mechanisms that cause the transformation into a turbid regime (Mohrig and Marr, 2003).

The critical Reynold's number, R_{ec}, describes a density flow as it becomes turbulent:

$$R_{ec} = \frac{U_c d_c}{\kappa} \qquad (3)$$

where U_c, d_c, κ are the critical velocity, flow thickness and kinematic viscosity. Laboratory studies were directed at estimating R_{ec} for subaqueous sediment slurries of different viscosities (Hampton, 1972; Table 1) and are supported by similar values derived from field data (e.g., Table 2 in Zeng et al., 1997). Next, we use an expression for laminar flow down an open channel,

$$U_c = \sqrt{\frac{8\rho' g d_c \sin(\alpha)}{f}} \text{,(Middleton, 1966)} \qquad (4)$$

where $\rho' = (\rho_{debris} - \rho_{water})/\rho_{debris}$, g is gravitational acceleration, $\alpha = tan(S_t)$, and f is the flow resistance factor. Based on assumptions (1) and (3), we combine eq. (4) with eq. (3) to solve for d_c as a function of the threshold-1 channel gradient. In other words, we can estimate the bounding conditions for critical flow thickness at the threshold in which flows becomes turbulent:

$$d_c = \varepsilon \sin(\alpha)^{-1/3}, \qquad (5)$$

Here, $\varepsilon = (R_{ec}\kappa)^{2/3}\left(\frac{8\rho' g}{f}\right)^{-1/3}$. R_{ec} estimates presented by Hampton (1972) were used to resolve a range of values for ε (Table 2), and Eq. (5) is solved for each measured

gradient, S_t, at threshold-1. Each critical thickness estimate, d_c, at threshold-1 has an associated catchment area. Using the mean and standard deviation for ε, an envelope of critical thickness values is determined by least-squares regression of d_c versus A_t (Figure 11): $d_c=(16.91 \pm 7.62)\cdot A_t^{0.06}$ ($R^2 = 0.72$).

Although this approach is based on several assumptions, the critical flow thickness in slope-sourced canyons is predicted to range between 15 – 85 m depending on the material properties assumed for the flow (e.g., shear strength). Debris flows sourced from smaller catchments traverse steeper slopes and, at the point of ignition, are expected to be thinner than flows from larger catchments. Debris flows are not expected to transform into turbidity flows during every failure event, only those capable of attaining the critical thickness needed for ignition. One possibility is that earthquakes trigger simultaneous and pervasive slope failures within canyon heads. The resulting debris flows converge within the landslide catchment and provide the volume and flux needed for flows to achieve critical thickness.

Following a seismic event, such as 1929 Grand Banks (Piper et al., 1999; Piper and Normark, 2009), canyons with greater catchment areas are expected to yield relatively greater volumes and fluxes of failed sediment. The hypothetical flow discharge at threshold-1 for such events can be estimated by multiplying the cross-sectional canyon area at a height d_c above the canyon thalwag by the critical velocity needed for ignition (Table 2). Depending on the boundary conditions set by ε and typical thalwag widths at threshold-1 (250–500 m for USAM and 100–150 m for Sur), flow discharge is calculated to range from 6,000–47,000 m^3/s for USAM and 2,000–10,500 m^3/s for Sur canyons. These estimates are in line with observations from natural flows (e.g., Table 2 of Zeng

and Lowe, 1997). In summary, quantitative analysis of geomorphic process boundaries in slope-sourced canyons may provide minimum bounds on the volume of sediment that is mobilized and transported to the deep sea during seismically triggered failures.

5.3. Implications of canyon-valley domains

Sediment entrainment/suspension models for rivers (Akiyama and Stefan, 1985) were applied to turbidity flows (Parker et al., 1986), suggesting that turbidity current morphodynamics in a graded canyon may be controlled by similar erosional processes as rivers. Though it may not be surprising that the range of intrinsic concavity for canyon-valley segments (0.3 – 0.7) is similar to that of fluvial systems (Mitchell, 2005), we do not fully understand the physical mechanisms that leads to these similarities. Sediment failures and steep gullies appear to be concentrated within the landslide domains (Twichell and Roberts, 1982; Piper and Normark, 2009), but they also occur along steep canyon walls down the entire length of canyons, meaning the cumulative volume of loose sediment supplied to canyon floors increases as a function of catchment area (analogous to increasing river discharge as a function of catchment area). If a turbidity flow remains supercritical (Froude number > 1), it's flux may be expected to increase as it travels down canyon and entrains water and loose sediment from the canyon floor (Gerber et al., 2009).

Along the USAM, θ_{A1} canyon segments are entrenched in the continental slope and may represent the steady-state profile for canyons formed primarily by highly erosive, supercritical turbidity flows (Mitchell, 2005) (Figure 10b). The change in concavity between θ_{A1} and θ_{A2} segments is not necessarily related to sudden changes in

thalwag gradient at the slope-rise transition (Garcia and Parker, 1989). In several canyons, it appears to be closely aligned with an abrupt decrease in canyon relief along the lower slope/upper rise (Figures 4, 8a–c). Canyon relief may have a profound influence on turbidity flow evolution, including the location of hydraulic jumps along the slope-rise transition (Garcia and Parker, 1989). As canyon relief decreases near the slope-rise transition, flows are allowed to spread laterally and decrease in thickness, inducing a change from an overall erosive to an overall depositional flow regime.

Mechanically, the transition to canyon segments marked by θ_{A2} and θ_{M1} may represent a transformation from super-critical to subcritical flow states (Figure 10b; Garcia and Parker, 1989). Subcritical turbidity flows transport sediment both in suspension and as bedload. Within this framework, bathymetric relief of canyons/channels dominated by subcritical turbidity flows would result from greater overbank and levee deposition than thalwag aggradation (Gerber et al., 2009). The θ_{A2} canyon segments may represent steady-state profiles of aggradational, levee-confined channels formed by sub-critical flows across the upper continental rise. In contrast, turbidity flows sourced from the short, steep landslides below the Sur Platform may not have sufficient discharge or steep enough gradients along θ_{M1} segments to maintain a supercritical state over long distances. Despite the low gradients, flows continue through the θ_{M1} segments because they entrain loose material sourced from local failures (Greene et al., 2002) and the flows are confined by relatively high and steep canyon walls, allowing them to maintain critical thickness. Finally, the segment of nearly flat concavity, θ_{A3}, is associated with very low gradients ($<< 1°$), deep-water distributary channels and, presumably, flow termination. Dramatic steepening and evidence for thalwag incision

down canyon of θ_{M3} (Figures 4d and 8d) suggests flows accelerate and perhaps return to a supercritical state across the lowermost slope.

A terrestrial analog for the submarine canyon segments dominated by critical versus subcritical flows may be the transitions between "transport limited" and "supply limited" conditions in river networks (Whipple and Tucker, 2002). The higher concavity and v-shaped cross sections of θ_{A1} segments suggests the transport capacity exceeds the canyon bed sediment supply. The θ_{A2} and θ_{M1} segments are associated with low gradients, and wide, flat-bottomed channels that may imply these segments are characterized by net aggradation of the channel floors and banks.

6. Conclusions

Although similarities between terrestrial and submarine terrain networks raise a number of philosophical questions regarding the true meaning of terrain derived power-laws (Straub et al., 2007), we believe such approaches can be used to (1) identify geomorphic process boundaries in either environment and (2) quantify some of the boundary conditions for sediment flows that are responsible for submarine canyon formation. The steep canyon heads along the uppermost continental slope appear to be the primary source regions for debris flows that disintegrate and transform into erosive turbidity flows. Once turbidity flows are generated, they can become self-accelerating through erosion and entrainment of loose sediment deposited along canyon floors, thus increasing in volume and erosivity in a way that is analogous to increasing discharge in river systems (Mitchell, 2005). Based on the patterns we observe, debris flows generated in canyon heads steeper than 4°–5° can transform into erosive turbidity flows as long as a

critical threshold in flow thickness is exceeded. Over geological timescales, the transformation of canyon-confined debris flows into turbidity flows appears to leave behind a predictable geomorphic fingerprint (e.g., Threshold-1). One possibility is that earthquakes trigger simultaneous and regionally pervasive slope failures (e.g., 1929 Grand Banks sequence of events; Piper et al., 1999) within canyon heads, thus yielding the critical volume and flux needed for debris flows to transform into turbidity flows.

Given the difficulties in obtaining *in situ* measurements of sediment flows, coupled with the ever-expanding volume of high-quality bathymetric data, continued efforts to develop terrain-based seascape erosion models are important. While many of the major shelf-sourced submarine canyons of the world play important roles in the geomorphic development of continental margins and in the growth of deep sea fan systems (Shepard, 1981), it is possible that the smaller, slope-sourced canyons are better suited for studies aimed at understanding relationships between form and process.

7. References

Adams, E.W., Schlager, W., 2000. Basic types of submarine slope curvature. Journal of Sedimentary Research 70, 814-828.

Akiyama, J., Stefan, H., 1985. Turbidity-Current with Erosion and Deposition. Journal of Hydraulic Engineering-Asce 111, 1473-1496.

Andrews, B.D., Chaytor, J.D., ten Brink, U.S., Brothers, D.S., Gardner, J.V., 2013. Bathymetric terrain model of the Atlantic Margin for marine geological investigations. U.S. Geological Survey Open-File Report.

Belderson, R.H., Stride, A.H., 1969. Shape of Submarine Canyon Heads Revealed by Asdic. Deep-Sea Research 16, 103-104.

Brothers, D.S., ten Brink, U.S., Andrews, B.D., Chaytor, J.D., 2013. Geomorphic characterization of the US Atlantic continental margin. Marine Geology in press.

Eittreim, S.L., Anima, R.J., Stevenson, A.J., 2002. Seafloor geology of the Monterey Bay area continental shelf. Marine Geology 181, 583-583.

Farre, J.A., McGregor, B.A., Ryan, W.B.F., Robb, J.M., 1983. Breaching the shelfbreak: passage from youthful to mature phase in submarine canyon evolution. SEPM, Tulsa, OK.

Galloway, W.E., 1998. Siliciclastic slope and base-of-slope depositional systems: Component facies, stratigraphic architecture, and classification. Aapg Bulletin 82, 569-595.

Garcia, M., Parker, G., 1989. Experiments on Hydraulic Jumps in Turbidity Currents near a Canyon-Fan Transition. Science 245, 393-396.

Gardner, W.D., 1989. Baltimore Canyon as a Modern Conduit of Sediment to the Deep-Sea. Deep-Sea Research Part a-Oceanographic Research Papers 36, 323-358.

Gerber, T.P., Amblas, D., Wolinsky, M.A., Pratson, L.F., Canals, M., 2009. A model for the long-profile shape of submarine canyons. Journal of Geophysical Research-Earth Surface 114, -.

Goff, J.A., 2001. Quantitative classification of canyon systems on continental slopes and a possible relationship to slope curvature. Geophysical Research Letters 28, 4359-4362.

Greene, H.G., Maher, N.M., Paull, C.K., 2002. Physiography of the Monterey Bay National Marine Sanctuary and implications about continental margin development. Marine Geology 181, 55-82.

Hampton, M.A., 1972. Role of subaqueous debris flows in generating turbidity currents. Journal of Sedimentary Petrology 42, 775-793.

Hatcher, G., Caress, D., Maher, N., Clague, D., Greene, G., Barr, N., 2000. Monterey Bay multibeam survey. Monterey Bay Aquarium Research Institute.

Howard, A.D., 1994. A detachment-limited model of drainage-basin evolution. Water Resources Research 30, 2261-2285.

Johnson, K.S., Paull, C.K., Barry, J.P., Chavez, F.P., 2001. A decadal record of underflows from a coastal river into the deep sea. Geology 29, 1019-1022.

Kennett, J.P., 1982. Marine Geology. Prentice Hall, Englewood Cliffs, NJ.

Kneller, B., Buckee, C., 2000. The structure and fluid mechanics of turbidity currents: a review of some recent studies and their geological implications. Sedimentology 47, 62-94.

Mcgregor, B., Stubblefield, W.L., Ryan, W.B.F., Twichell, D.C., 1982. Wilmington-Submarine Canyon - a marine fluvial-like system. Geology 10, 27–30.

Middleton, G.V., 1966. Experiments on density and turbidity currents II: uniform flow of density currents. Canadian Journal of Earth Sciences 3, 627–637.

Mitchell, N.C., 2004. Form of submarine erosion from confluences in Atlantic USA continental slope canyons. American Journal of Science 304, 590-611.

Mitchell, N.C., 2005. Interpreting long-profiles of canyons in the USA Atlantic continental slope. Marine Geology 214, 75-99.

Mitchell, N.C., Huthnance, J.M., 2007. Comparing the smooth, parabolic shapes of interfluves in continental slopes to predictions of diffusion transport models. Marine Geology 236, 189-208.

Mohrig, D., Marr, J.G., 2003. Constraining the efficiency of turbidity current generation from submarine debris flows and slides using laboratory experiments. Marine and Petroleum Geology 20, 883-899.

Mohrig, D., Whipple, K.X., Hondzo, M., Ellis, C., Parker, G., 1998. Hydroplaning of subaqueous debris flows. Geological Society of America Bulletin 110, 387-394.

Mosher, D., Piper, D., 2007. Analysis of multibeam seafloor imagery of the Laurentian Fan and the 1929 Grand Banks landslide area, in: Lykousis, V., Sakellariou, D., Locat, J. (Eds.), Submarine Mass Movements and Their Consequences. Springer, Amsterdam, pp. 77-88.

Mulder, T., Syvitski, J.P.M., 1995. Turbidity currents generated at river mouths during exceptional discharges to the world oceans. Journal of Geology 103, 285–299.

Parker, G., Fukushima, Y., Pantin, H.M., 1986. Self-accelerating turbidity currents. Journal of Fluid Mechanics 171, 145–181.

Paull, C.K., Caress, D., Lundsten, E., Gwiazda, R., Anderson, K., McGann, M., Conrad, J., Edwards, B.D., Sumner, E.J., 2013. Anatomy of the La Jolla Submarine Canyon system; offshore southern California. Marine Geology 334, 16–34.

Paull, C.K., Caress, D.W., Ussler, W., Lundsten, E., Meiner-Johnson, M., 2011. High-resolution bathymetry of the axial channels within Monterey and Soquel submarine canyons, offshore central California. Geosphere 7, 1077-1101.

Paull, C.K., Ussler, W., Greene, H.G., Keaten, R., Mitts, P., Barry, J., 2003. Caught in the act: the 20 December 2001 gravity flow event in Monterey Canyon. Geo-Marine Letters 22, 227-232.

Piper, D.J.W., Cochonat, P., Morrison, M.L., 1999. The sequence of events around the epicentre of the 1929 Grand Banks earthquake: initiation of debris flows and turbidity current inferred from sidescan sonar. Sedimentology 46, 79-97.

Piper, D.J.W., Normark, W.R., 2009. Processes that initiate turbidity currents and their influence on turbidites: a marine geology perspective. Journal of Sedimentary Research 79, 347–362.

Piper, D.J.W., Savoye, B., 1993. Processes of Late Quaternary Turbidity-Current Flow and Deposition on the Var Deep-Sea Fan, North-West Mediterranean-Sea. Sedimentology 40, 557-582.

Pirmez, C., Imran, J., 2003. Reconstruction of turbidity currents in Amazon Channel. Marine and Petroleum Geology 20, 823-849.

Pirmez, C., Pratson, L.F., Steckler, M.S., 1998. Clinoform development by advection-diffusion of suspended sediment: Modeling and comparison to natural systems. Journal of Geophysical Research-Solid Earth 103, 24141-24157.

Pratson, L.F., Coakley, B.J., 1996. A model for the headward erosion of submarine canyons induced by downslope-eroding sediment flows. Geological Society of America Bulletin 108, 225-234.

Pratson, L.F., Ryan, W.B.F., 1996. Automated drainage extraction in mapping the Monterey Submarine Drainage System, California margin. Marine Geophysical Researches 18, 757-777.

Pratson, L.F., Ryan, W.B.F., Mountain, G.S., Twichell, D.C., 1994. Submarine-canyon initiation by downslope-eroding sediment flows - evidence in Late Cenozoic strata on the New-Jersey continental slope. Geological Society of America Bulletin 106, 395–412.

Puig, P., Ogston, A.S., Mullenbach, B.L., Nittrouer, C.A., Parsons, J.D., Sternberg, R.W., 2004. Storm-induced sediment gravity flows at the head of the Eel submarine canyon, northern California margin. Journal of Geophysical Research-Oceans 109.

Ramsey, L.A., Hovius, N., Lague, D., Liu, C.S., 2006. Topographic characteristics of the submarine Taiwan orogen. Journal of Geophysical Research-Earth Surface 111.

Seidl, M.A., Dietrich, W.E., 1992. The problem of channel erosion into bedrock. Catena Suppl. 23, 101124.

Shepard, F.P., 1981. Submarine canyons: multiple causes and long-time persistence. Aapg Bulletin 65, 1062–1077.

Shepard, F.P., Emery, K.O., 1973. Congo Submarine Canyon and Fan Valley. American Association of Petroleum Geologists Bulletin 57, 1679–1691.

Stock, J., Dietrich, W.E., 2003. Valley incision by debris flows: Evidence of a topographic signature. Water Resources Research 39.

Straub, K.M., Jerolmack, D.J., Mohrig, D., Rothman, D.H., 2007. Channel network scaling laws in submarine basins. Geophysical Research Letters 34.

Streeter, V.L., Wylie, E.B., Bedford, K.W., 1998. Fluid mechanics, 9th ed. WCB/McGraw Hill, Boston.

ten Brink, U.S., Barkan, R., Andrews, B.D., Chaytor, J.D., 2009. Size distributions and failure initiation of submarine and subaerial landslides. Earth and Planetary Science Letters 287, 31-42.

Tucker, G.E., Bras, R.L., 1998. Hillslope processes, drainage density, and landscape morphology. Water Resources Research 34, 2751-2764.

Tucker, G.E., Whipple, K.X., 2002. Topographic outcomes predicted by stream erosion models: Sensitivity analysis and intermodel comparison. Journal of Geophysical Research-Solid Earth 107.

Twichell, D.C., Roberts, D.G., 1982. Morphology, distribution, and development of submarine canyons on the United-States Atlantic continental-slope between Hudson and Baltimore canyons. Geology 10, 408-412.

Whipple, K.X., Tucker, G.E., 2002. Implications of sediment-flux-dependent river incision models for landscape evolution. Journal of Geophysical Research-Solid Earth 107.

Willgoose, G., Bras, R.L., Rodriguez-Iturbe, I., 1991a. A coupled channel network growth and hillslope evolution model .1. Theory. Water Resources Research 27, 1671-1684.

Willgoose, G., Bras, R.L., Rodriguez-Iturbe, I., 1991b. A physical explanation of an observed link area-slope relationship. Water Resources Research 27, 1697-1702.

Wobus, C., Whipple, K.X., kirby, E., Snyder, N.P., Johnson, J., Spyropolou, K., Crosby, B.T., Sheehan, D., 2006. Tectonics from topography: procedures, promise, and pitfalls. Geological Society of America Special Paper 398, 55-74.

Wong, F.L., Eittreim, S.L., 2002. Continental shelf GIS for the Monterey Bay National Marine Sanctuary. Marine Geology 181, 317-321.

Xu, J.P., Noble, M.A., Rosenfeld, L.K., 2004. In-situ measurements of velocity structure within turbidity currents. Geophysical Research Letters 31.

Zeng, J.J., Lowe, D.R., 1997. Numerical simulation of turbidity current flow and sedimentation .1. Theory. Sedimentology 44, 67-84.

Acknowledgements

We thank the USGS Mendenhall Postdoctoral Fellowship Program and the U.S. Nuclear Regulatory Commission for supporting this work. We also thank N. Mitchell, L. Brothers and J. Denny for helpful reviews. Neither the U.S. Government, the Department of the Interior, nor the USGS, nor any of their employees, contractors, or subcontractors, make any warranty, express or implied, nor assume any legal liability or responsibility for the accuracy, completeness, or usefulness of any information, apparatus, product, or process disclosed, nor represent that its use would not infringe on privately owned rights. The act of distribution shall not constitute any such warranty, and no responsibility is assumed by the USGS in the use of these data or related materials. Any use of trade, product, or firm names is for descriptive purposes only and does not imply endorsement by the U.S. Government.

Table and Figure Captions

Table 1. Summary of power law scaling parameters estimated for canyons of US Atlantic Margin and the Monterey Margin.

Table 2. Laboratory-based measurements of mud slurries as they transition from a laminar or near laminar flow state to a turbulent regime (data from Table 1 of Hampton, 1972). Parameter ε is used in the present study to estimate the critical flow thickness of canyon-confined debris flows as they are ignited into turbidity flows (Figure 11).

$\varepsilon = \left(R_{ec}\kappa\right)^{2/3}\left(\frac{8\rho' g}{f}\right)^{-1/3}$, where κ = kinematic viscosity, R_{ec}= critical Reynolds number, U_c= critical velocity, $\rho' = \left(\rho_{debris} - \rho_{water}\right)/\rho_{debris}$, g = 9.8 m/s, and the flow resistance factor, f, was set at a constant value of 0.3 based on work by Middleton (1966). Note a scaling factor of 4 is applied to R_{ec} values from Hampton (1972) to convert from pipe flow to semi-circular channel flow (Streeter et al., 1998).

Figure 1. Regional shaded relief maps for the US Atlantic Margin (USAM; **a**) and the Monterey Margin of central California (**b**) based on multibeam bathymetry data (darker shades) merged with NOAA's U.S. Coastal Relief Model (lighter shades). Initially, all submarine canyons and channels (blue lines in panels **c** and **d**) were extracted from bathymetric DEMs. Red boxes are locations of subsequent figures. All contours have 500 m vertical spacing.

Figure 2. Hypothetical thalwag profile and associated topographic signatures for a terrestrial channel network. Catchment area (A) and channel gradient (S) are measured at discreet points along a stream profile (**a**) and plotted in log-log space to examine power-law scaling parameters (**b**; based on Whipple and Tucker [1999; 2002]; Stock and

Dietrich [2003]). Soil creep, debris flows and landslides dominate erosion in steep channel-heads where catchment area is less than ~1 km^2 (dashed line). Increasing fluvial discharge down stream is the dominant erosion mechanism in the channel-valley domains (solid black line).

Figure 3. Canyon relief map of the New England margin adjacent to Powell Canyon, one of the major shelf-breaching canyon systems of the USAM (see Figure 1 for regional location). An interpolated surface that connects inter-canyon ridges is used as a hypothetical un-canyonized DEM. Canyon relief is measured as the vertical difference between the un-canyonized surface and the true bathymetry. Bold, black line above canyon heads (red dots) represents the drainage divide. Bathymetric contours are marked every 200 m.

Figure 4. Examples of characteristic slope-sourced canyon profiles for the USAM (**a**) and the Monterey (**b**) margin. Top panels: depth versus distance downslope for canyon thalwags (colored lines) and hypothetical canyon interfluves (black lines). Middle panels: thalwag gradient and relief versus distance downslope. Bottom panels: *S-A* plots illustrating the regression segments determined for various canyon reaches. Threshold-1 marks the transition from "landslide" dominated morphology to "canyon-valleys", i.e., where canyons change from having linear or convex profiles to concave profiles.

Figure 5. Geomorphic comparison of two slope-sourced canyons along the New England margin (see Figure 1 for location). (**a**) Shaded relief overlain by canyon networks. The

two canyons selected illustrate differences between (1) long and narrow versus short and wide landslide domain catchments (green regions and red lines; orange lines represent canyon segments within the canyon-valley domain). (**b**) Bathymetric profiles. (**c**) Catchment area versus distance from divide. (**d**) *S-A* plots. Threshold-1 (white circles) occurs at approximately the same catchment area in both canyons, but at substantially different depths (1100 m versus 1700 m) and distances from the drainage divide (5 km versus 11 km).

Figure 6. Summary of regression analysis and threshold-1 picks for all slope-sourced canyons along the USAM (**a**) and the Sur Platform (**b**). Colored segments represent average values of the regression analyses applied to each individual canyon. The median Threshold-1 value for each margin is shown as a white dot and the range of associated S_t and A_t values as a cross-hair (see text for explanation). Regression analysis for segment θ_{M3} was not attempted due to its highly variably nature. (**c**) Log-log plot of Threshold-1 values for the US Atlantic Margin and the Sur Platform canyons. Regression analysis was applied separately to data from each margin and to the combined dataset.

Figure 7. Three-dimensional views of fine-scale seafloor morphology along the Mid-Atlantic slope (**a**; see Figure 1 for locations) and below the Sur Platform (**b**). Canyon segments are colored according to their intrinsic concavities, θ_i. Blue lines are debris flow channels, red lines are slide scars. θ_{LS} denotes the landslide segments of the canyons. Bathymetric data are gridded at 10-m and 5-m resolution for (a) and (b), respectively.

Figure 8. Shaded-relief maps of slope-sourced submarine canyons along the US Atlantic Margin (**a–c**) and along the Sur Platform of the Monterey Margin (**d**). See Figure 1 for regional locations. The black line along upper slope represents the hypothetical drainage divide (e.g., Figure 3). Canyon thalwags are colored according to their associated *S-A* scaling parameter, θ_i (e.g., Figures 4, 6 and 10; see [d] for legend). For each canyon, threshold-1 is located at the downslope termination of the landslide canyon segment (red lines). Blue arrows are locations of canyons shown in Figure 4. Contours are every 500 m.

Figure 9. Shaded relief imagery for canyons along (**a**) the New England margin and (b) the Sur Platform (see Figure 1 for locations). The colored lines correspond to intrinsic concavity segments determined from gradient-area analysis (e.g., Figure 6). Bathymetric cross-sections were extracted and plotted for two canyons along each margin to illustrate the down-slope variation in cross-sectional form.

Figure 10. (**a**) Hypothetical longitudinal canyon profile and associated morphological domains for a slope-sourced submarine canyon. (**b**) A summary of interpreted *S-A* regression segments (See Figure 6 and Table 1), but excluding canyon segments of extreme variation and convexity, such as along the lower slope of the Sur Platform.

Figure 11. Predicted thickness envelope for slope-sourced debris flows, d_c, as they transform into turbidity flows as a function of catchment area, A. The three curves

represent a range of d_c values that correspond to differences in material properties of debris flows (see text for details).

Margin	Number of Canyons	Threshold-1 (S_t, A_t)		Canyon-valley Segments Mean Concavities	
		Median Gradient	Median Area	1st Segment	2nd Segment
US Atlantic	120	7.3°	8.8 km^2	$\theta_{A1} = 0.65 \pm 0.06$	$\theta_{A2} = 0.39 \pm 0.07$
Monterey, CA	51	11.3°	0.4 km^2	$\theta_{M1} = 0.44 \pm 0.05$	$\theta_{M2} = < 0.1$

Laboratory measurements for mud slurries (data from Table 1 of Hampton, 1972)

κ (Pa·s)	U_c (m/s)	ρ'	R_{ec}	ε
0.0223	4.89	0.17	54000	32.17
0.0223	4.73	0.17	78400	41.25
0.0223	4.33	0.17	11840	11.70
0.0223	4.48	0.17	24560	19.03
0.0223	4.12	0.17	44400	28.23
0.0223	4.21	0.17	69200	37.95
0.0163	3.66	0.15	13440	10.64
0.0163	3.94	0.15	29000	17.76
0.0163	3.36	0.15	49600	25.40
0.0163	3.51	0.15	77600	34.24
0.0149	3.36	0.14	26640	16.35
0.0149	2.75	0.14	43600	22.71
0.0149	2.9	0.14	68800	30.78
0.0119	2.35	0.13	11520	8.20
0.0119	2.41	0.13	23640	13.24
0.0119	2.32	0.13	45600	20.52
0.0119	2.35	0.13	69200	27.10
0.0089	1.65	0.11	10560	6.81
0.0089	1.62	0.11	20720	10.67
0.0089	1.55	0.11	39680	16.45
0.0089	1.55	0.11	59600	21.58

Mean	3.24	0.14	40958	21.56
Stdev	1.17	0.02	22470	9.71

Figure 1

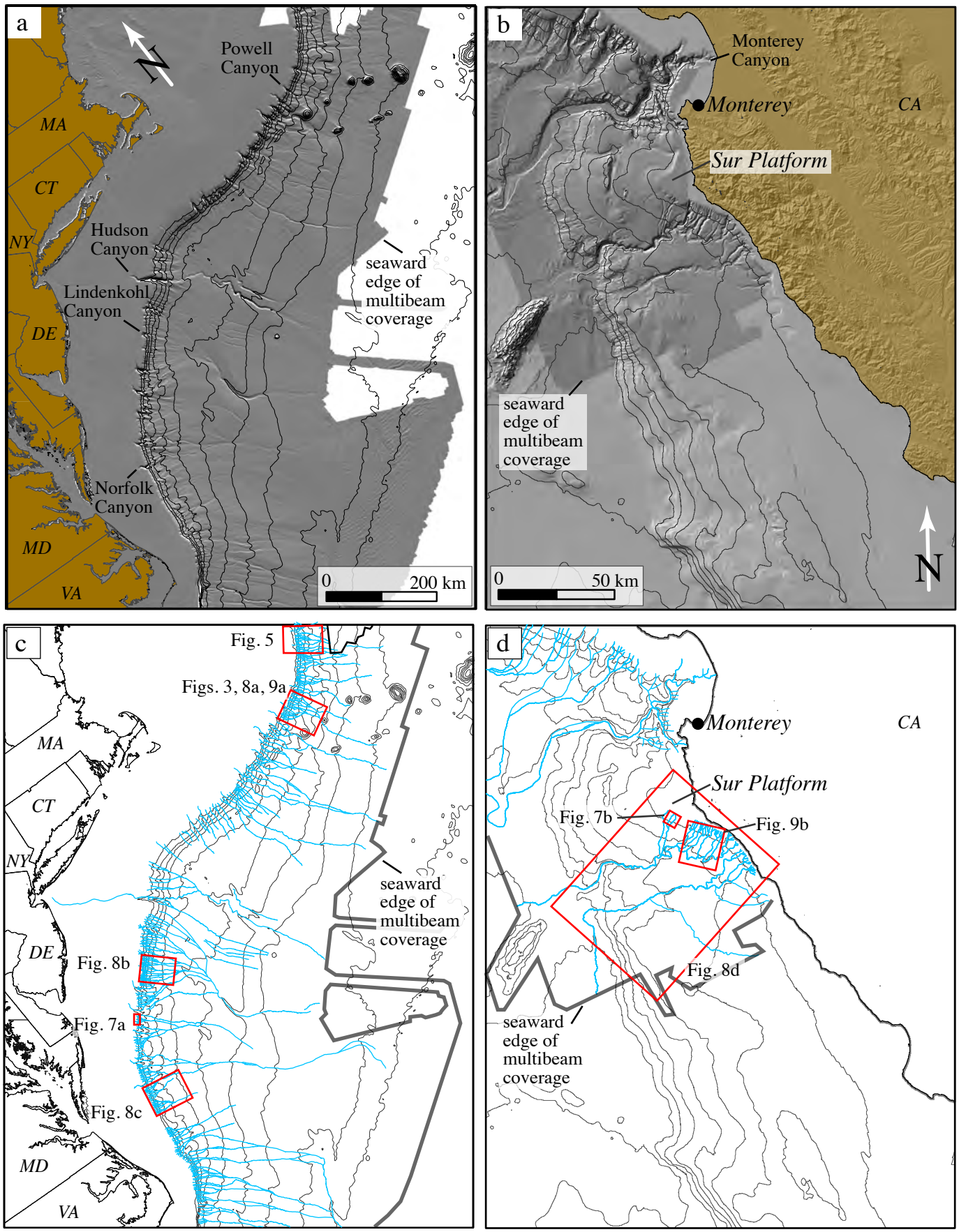
a
N
Powell Canyon
MA
CT
NY
Hudson Canyon
Lindenkohl Canyon
DE
seaward edge of multibeam coverage
Norfolk Canyon
MD
VA
0
200 km
b
Monterey Canyon
Monterey
CA
Sur Platform
seaward edge of multibeam coverage
0
50 km
N
c
Fig. 5
Figs. 3, 8a, 9a
MA
CT
NY
seaward edge of multibeam coverage
DE
Fig. 8b
Fig. 7a
Fig. 8c
MD
VA
d
Monterey
CA
Sur Platform
Fig. 7b
Fig. 9b
Fig. 8d
seaward edge of multibeam coverage

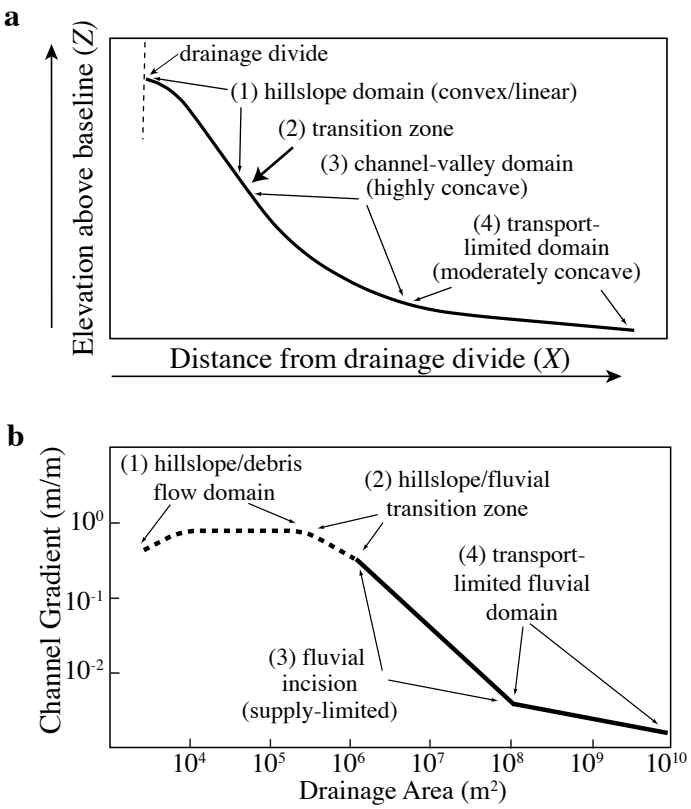
a
Elevation above baseline (Z)
drainage divide
(1) hillslope domain (convex/linear)
(2) transition zone
(3) channel-valley domain
(highly concave)
(4) transport-
limited domain
(moderately concave)
Distance from drainage divide (X)
b
Channel Gradient (m/m)
(1) hillslope/debris
flow domain
(2) hillslope/fluvial
transition zone
(4) transport-
limited fluvial
domain
(3) fluvial
incision
(supply-limited)
10^0
10^-1
10^-2
10^4
10^5
10^6
10^7
10^8
10^9
10^10
Drainage Area (m^2)

Figure 2

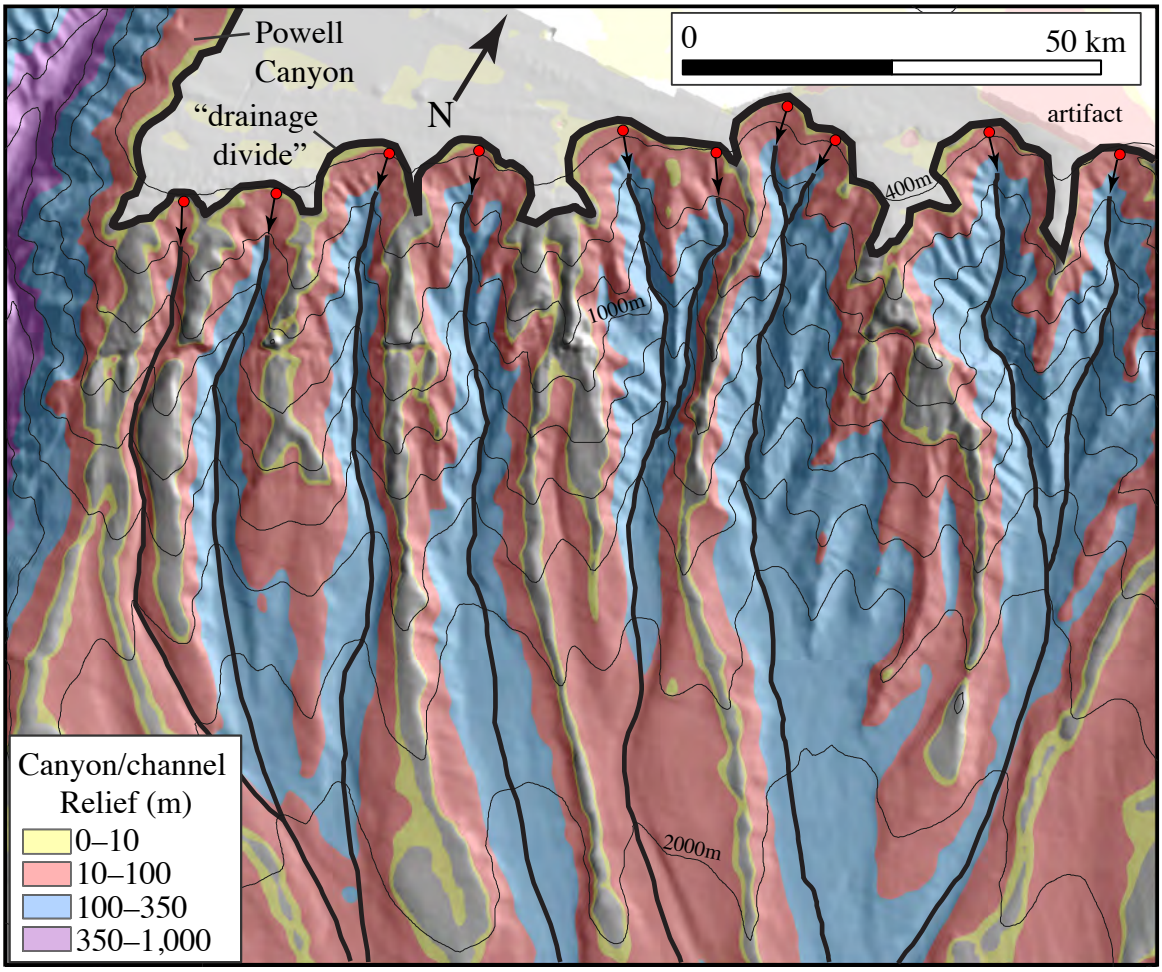
Powell
Canyon
"drainage
divide"
N
0
50 km
artifact
400m
1000m
2000m
Canyon/channel
Relief (m)
0–10
10–100
100–350
350–1,000

Figure 3

Figure 4

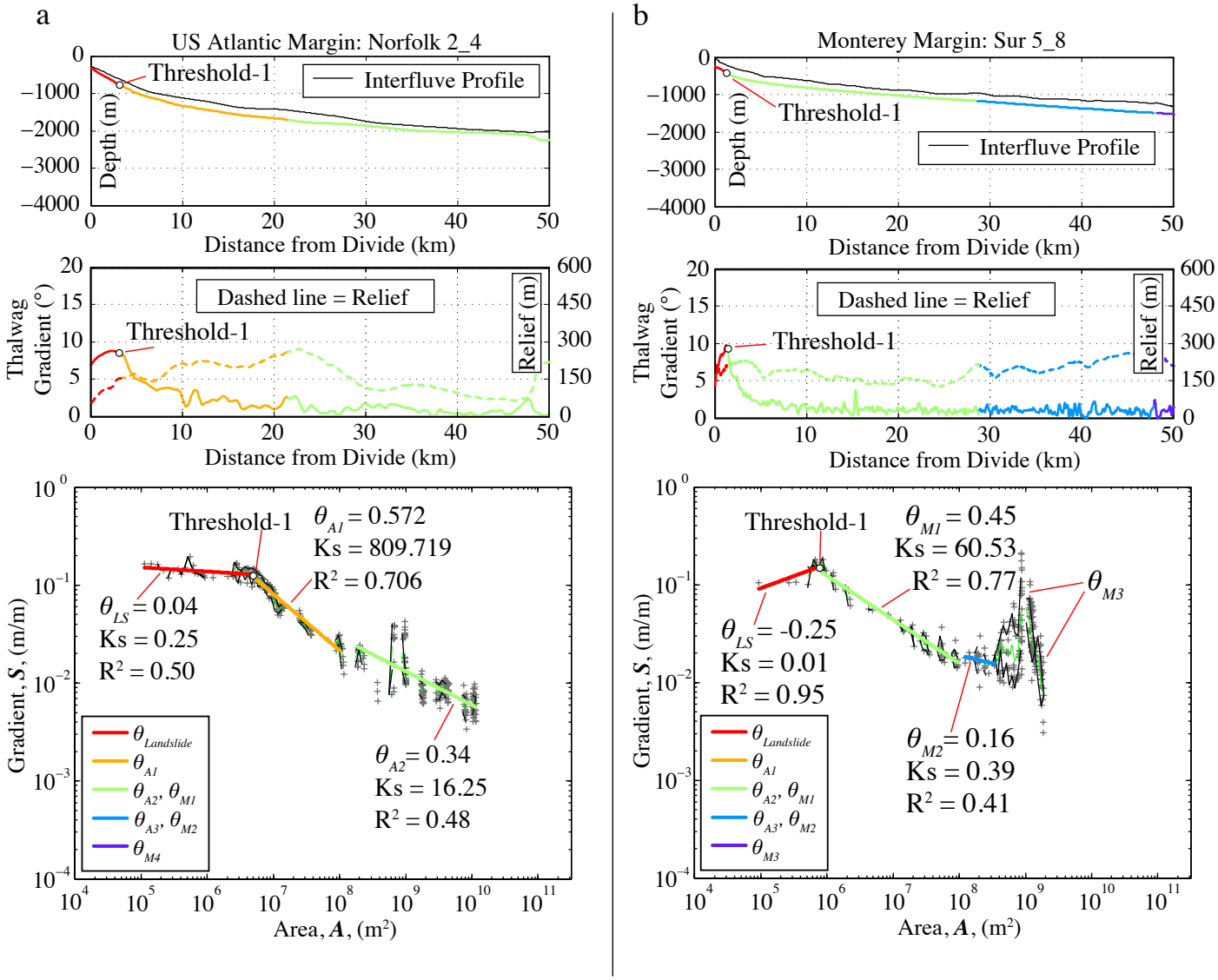
a
US Atlantic Margin: Norfolk 2_4
Threshold-1
Interfluve Profile
Depth (m)
Distance from Divide (km)
Dashed line = Relief
Thalwag Gradient (°)
Relief (m)
Gradient, S, (m/m)
Area, A, (m²)
θLS = 0.04
Ks = 0.25
R² = 0.50
θA1 = 0.572
Ks = 809.719
R² = 0.706
θA2 = 0.34
Ks = 16.25
R² = 0.48
θLandslide
θA1
θA2, θM1
θA3, θM2
θM4
b
Monterey Margin: Sur 5_8
θM1 = 0.45
Ks = 60.53
R² = 0.77
θM3
θLS = -0.25
Ks = 0.01
R² = 0.95
θM2 = 0.16
Ks = 0.39
R² = 0.41

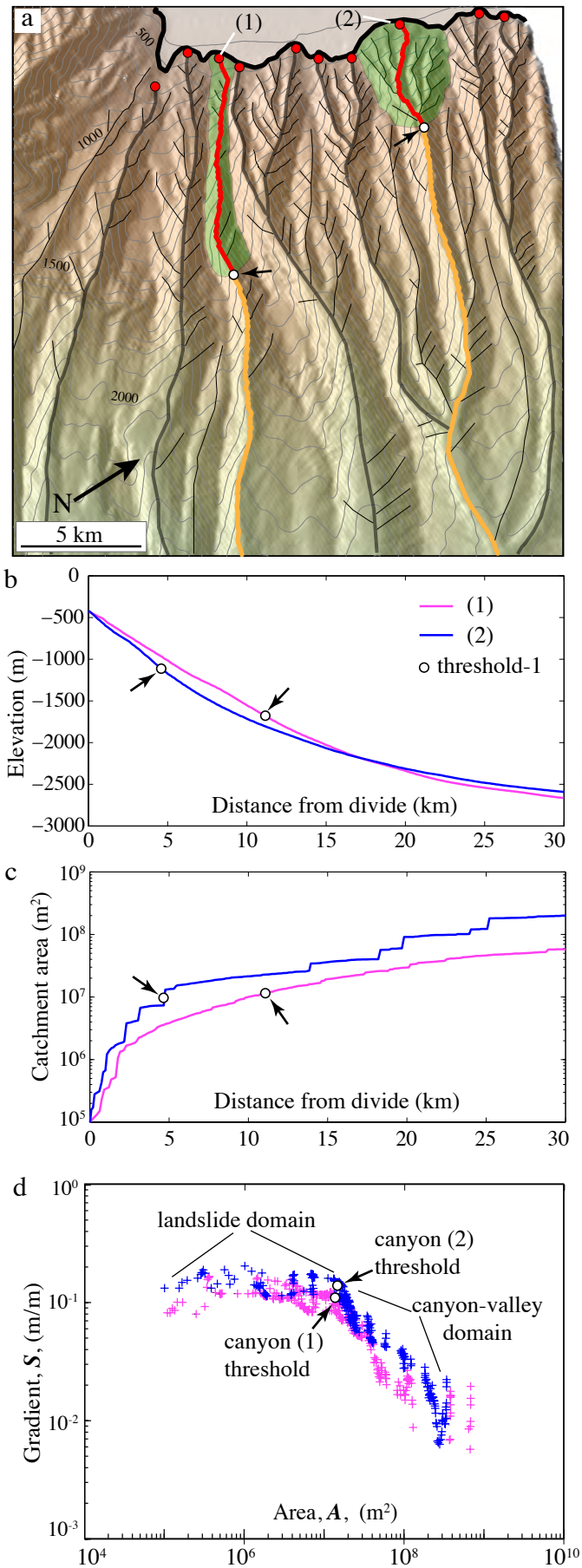
a
(1)
(2)
500
1000
1500
2000
N
5 km
b
Elevation (m)
Distance from divide (km)
(1)
(2)
threshold-1
c
Catchment area (m²)
Distance from divide (km)
d
Gradient, S, (m/m)
Area, A, (m²)
landslide domain
canyon (2) threshold
canyon-valley domain
canyon (1) threshold

Figure 5

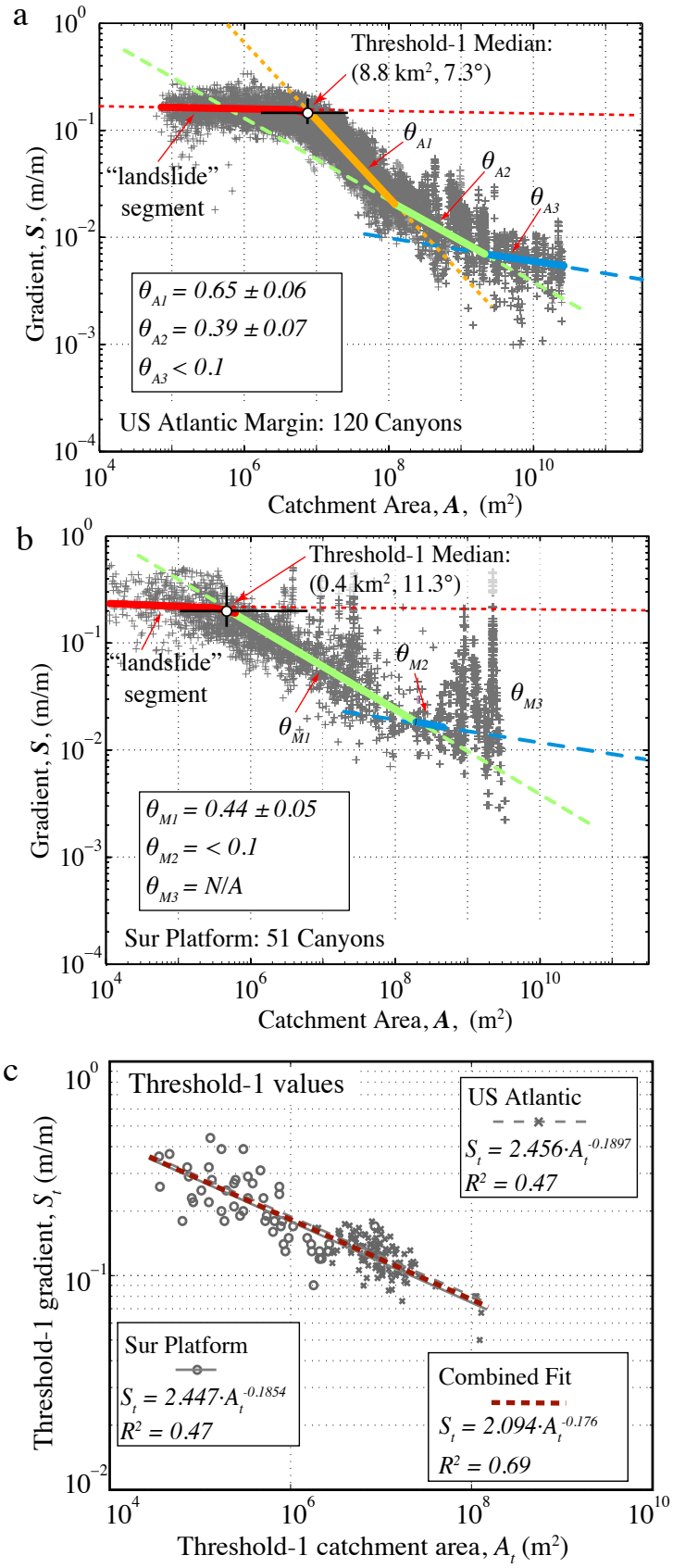
a
Threshold-1 Median:
(8.8 km², 7.3°)
"landslide"
segment
θA1
θA2
θA3
θA1 = 0.65 ± 0.06
θA2 = 0.39 ± 0.07
θA3 < 0.1
US Atlantic Margin: 120 Canyons
Gradient, S, (m/m)
Catchment Area, A, (m²)
b
Threshold-1 Median:
(0.4 km², 11.3°)
"landslide"
segment
θM1
θM2
θM3
θM1 = 0.44 ± 0.05
θM2 = < 0.1
θM3 = N/A
Sur Platform: 51 Canyons
Gradient, S, (m/m)
Catchment Area, A, (m²)
c
Threshold-1 values
US Atlantic
St = 2.456·At^-0.1897
R² = 0.47
Sur Platform
St = 2.447·At^-0.1854
R² = 0.47
Combined Fit
St = 2.094·At^-0.176
R² = 0.69
Threshold-1 gradient, St (m/m)
Threshold-1 catchment area, At (m²)

Figure 6

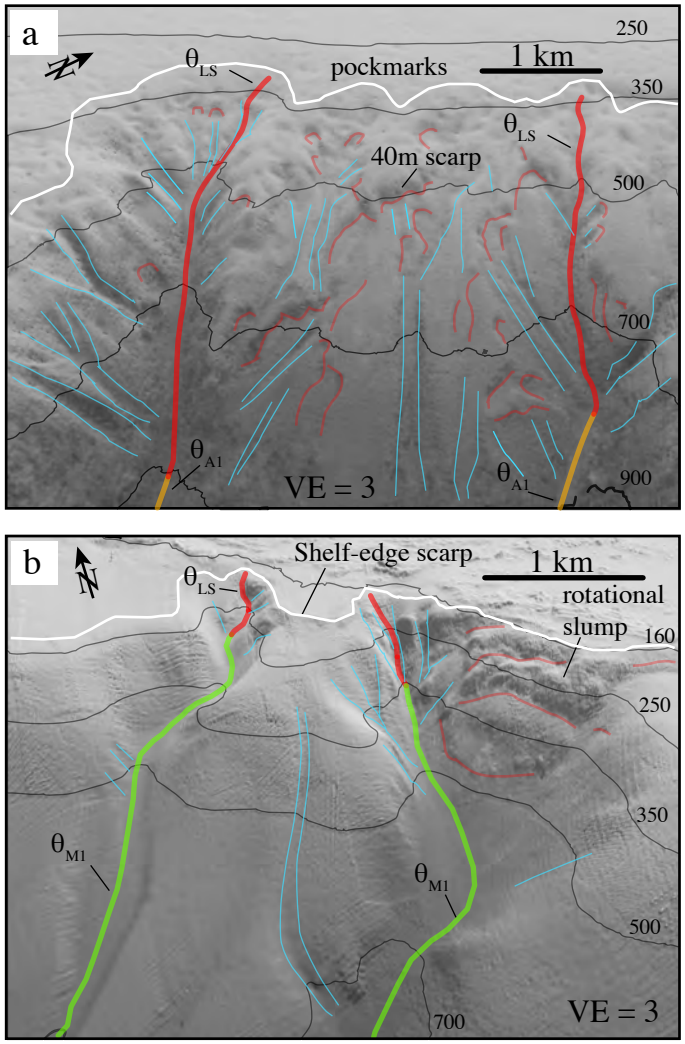
a
N
θLS
pockmarks
1 km
250
350
θLS
40m scarp
500
700
θA1
VE = 3
θA1
900
b
N
θLS
Shelf-edge scarp
1 km
rotational
slump
160
250
350
θM1
θM1
500
700
VE = 3

Figure 7

Figure 8

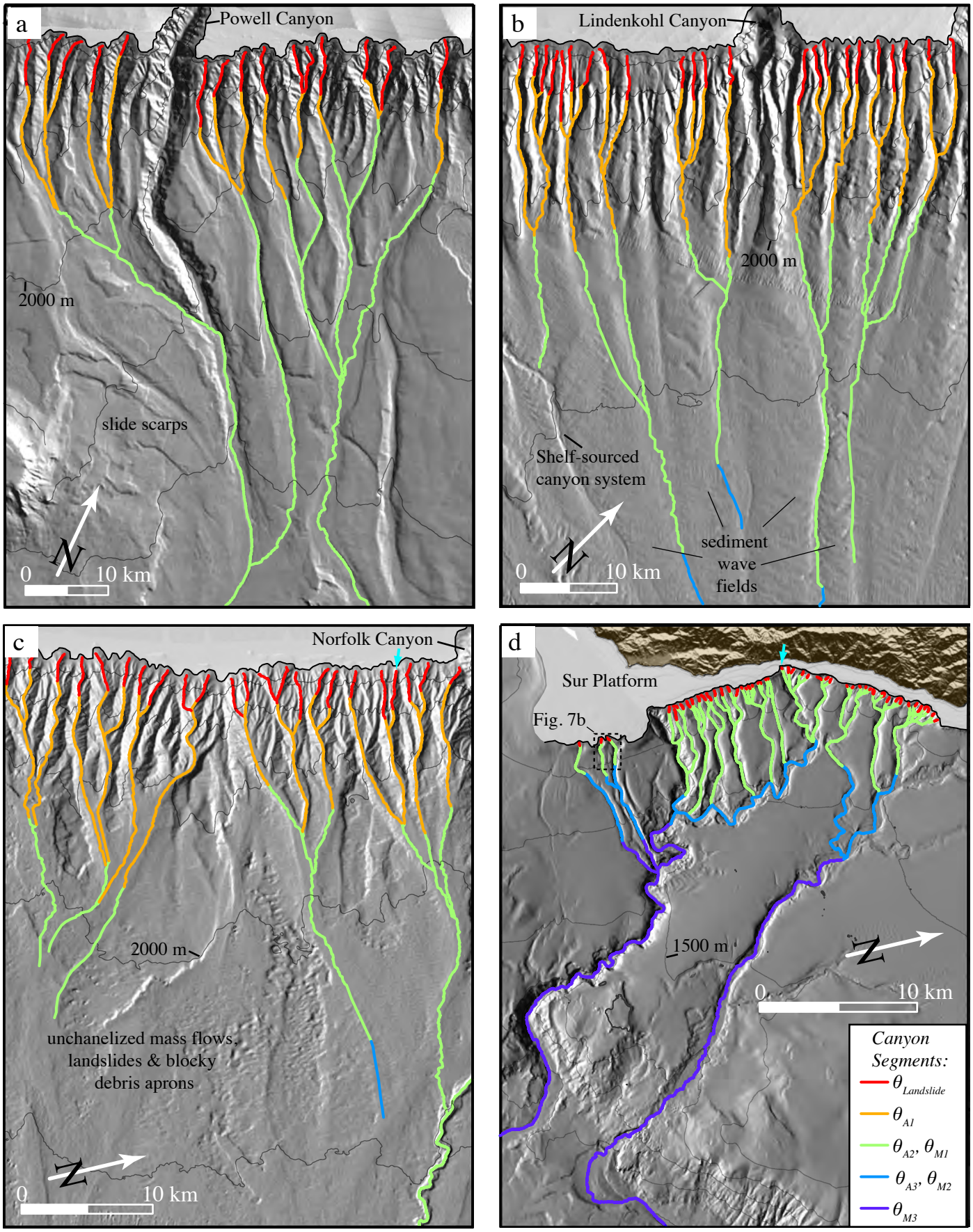
a
Powell Canyon
2000 m
slide scarps
N
0
10 km
b
Lindenkohl Canyon
2000 m
Shelf-sourced
canyon system
sediment
wave
fields
N
0
10 km
c
Norfolk Canyon
2000 m
unchanelized mass flows,
landslides & blocky
debris aprons
N
0
10 km
d
Sur Platform
Fig. 7b
1500 m
N
0
10 km
Canyon
Segments:
$\theta_{Landslide}$
θ_{A1}
θ_{A2}, θ_{M1}
θ_{A3}, θ_{M2}
θ_{M3}

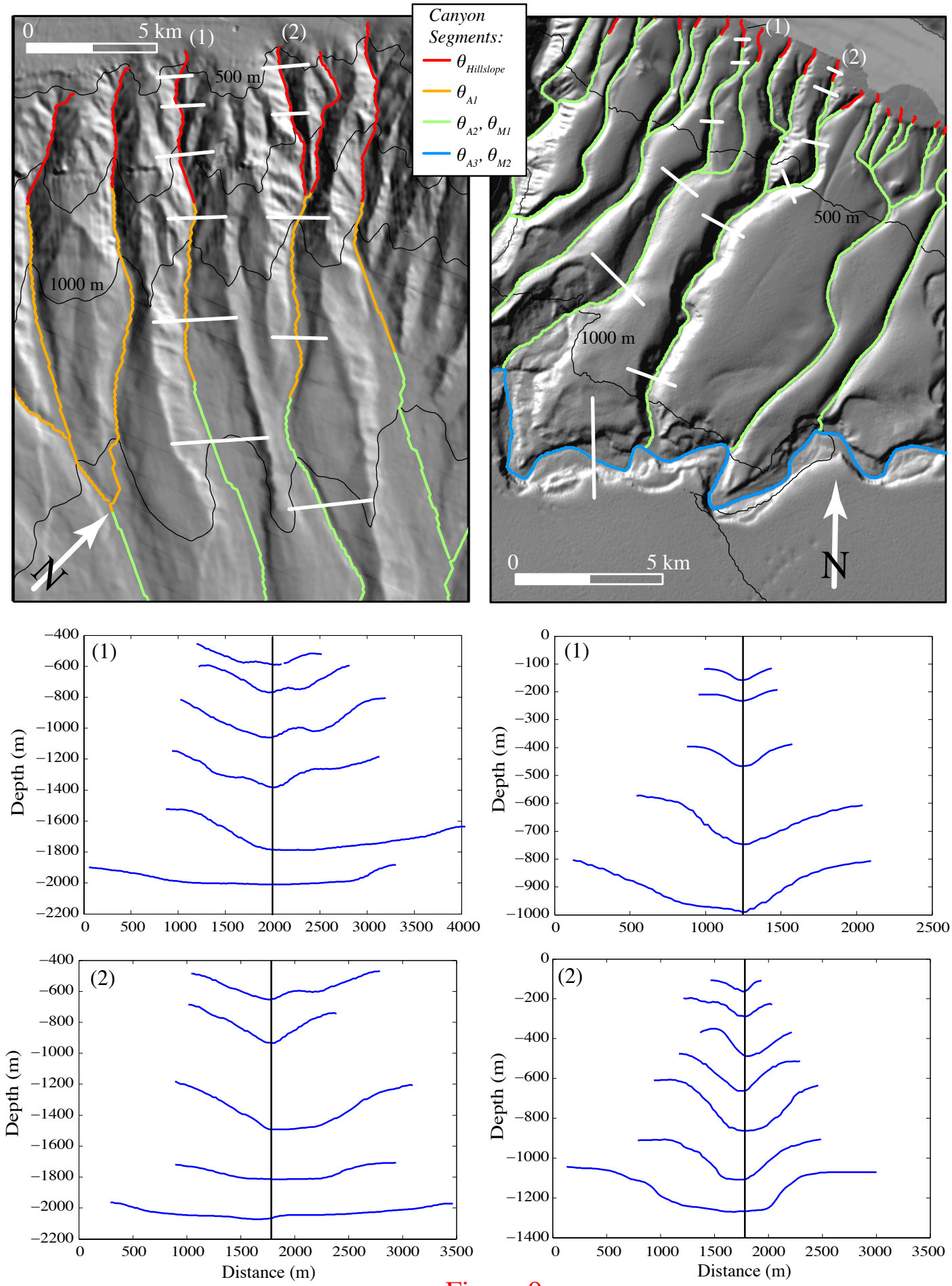
Canyon Segments:
$\theta_{Hillslope}$
θ_{A1}
θ_{A2}, θ_{M1}
θ_{A3}, θ_{M2}
0
5 km
(1)
(2)
500 m
1000 m
N
Depth (m)
Distance (m)

Figure 9

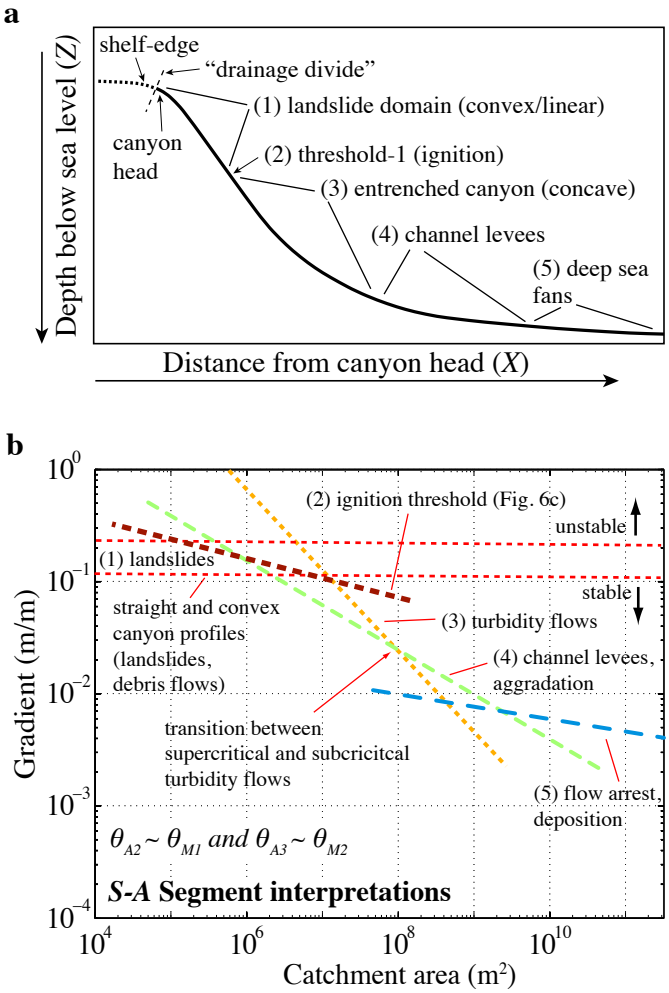
a
shelf-edge
"drainage divide"
(1) landslide domain (convex/linear)
canyon head
(2) threshold-1 (ignition)
(3) entrenched canyon (concave)
(4) channel levees
(5) deep sea fans
Depth below sea level (Z)
Distance from canyon head (X)
b
(2) ignition threshold (Fig. 6c)
unstable
(1) landslides
stable
straight and convex canyon profiles (landslides, debris flows)
(3) turbidity flows
(4) channel levees, aggradation
transition between supercritical and subcricitcal turbidity flows
(5) flow arrest, deposition
θA2 ~ θM1 and θA3 ~ θM2
S-A Segment interpretations
Gradient (m/m)
Catchment area (m2)

Figure 10

a

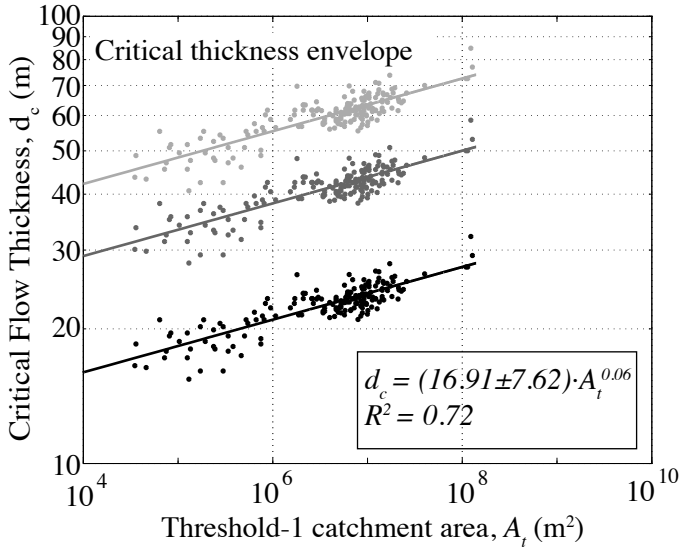
Critical thickness envelope
$d_c = (16.91 \pm 7.62) \cdot A_t^{0.06}$
$R^2 = 0.72$
Critical Flow Thickness, d_c (m)
Threshold-1 catchment area, A_t (m^2)
100
90
80
70
60
50
40
30
20
10
10^4
10^6
10^8
10^{10}

Figure 11